



PERGAMON

Deep-Sea Research I 49 (2002) 1531–1549

DEEP-SEA RESEARCH  
PART I

www.elsevier.com/locate/dsr

## The Reddy maker

Doron Nof<sup>a,\*</sup>, Nathan Paldor<sup>b</sup>, Stephen Van Gorder<sup>a</sup>

<sup>a</sup>Department of Oceanography 4320, The Florida State University, Tallahassee, FL 32306-4320, USA

<sup>b</sup>Atmospheric Sciences, The Hebrew University of Jerusalem, Jerusalem 91904, Israel

Received 19 July 2001; received in revised form 6 June 2002; accepted 6 June 2002

### Abstract

A new mechanism for the formation of high-amplitude anticyclonic eddies (lenses) from outflows emptying into the ocean at mid-depth is proposed. The essence of the new mechanism is that, in order for an inviscid outflow to exist as a continuous (uninterrupted) current, the condition  $g'S/f > \alpha(g'H)^{1/2}$  [where  $g'$  is the “reduced gravity”,  $S$  the bottom slope,  $f$  the Coriolis parameter,  $\alpha$  a coefficient of order unity whose value depends on the outflow’s potential vorticity (it is  $\sqrt{2}$  for a zero potential vorticity outflow and unity for a uniform potential vorticity) and  $H$  the maximum thickness] must hold. When the above condition is not met, i.e., when  $g'S/f < \alpha(g'H)^{1/2}$ , the outflow can only exist as a chain of propagating lenses.

Nonlinear analytical considerations leading to the above conclusion are (successfully) compared to numerical simulations which we have conducted (using a reduced gravity layer-and-a-half model). The experiments show that an outflow situated on a bottom whose (uniform) slope gradually varies in the downstream direction is continuous (i.e., is not broken into eddies) where the slope is supercritical [ $g'S/f > \alpha(g'H)^{1/2}$ ] and discontinuous (i.e., constitutes a chain of eddies) where the slope is subcritical [ $g'S/f < \alpha(g'H)^{1/2}$ ]. Hence, the eddies are generated by the gradual reduction in the bottom slope rather than by an instability process. Namely, the eddies are not formed by the breakdown of a known steady solution because such a steady solution does not exist.

We note that after reaching its “balanced depth”, an outflow usually continues to (slowly) descend toward the bottom of the ocean due to frictional effects associated with an energy loss. [Note that the “balanced depth” is the depth at which the outflow has completed its initial adjustment in the sense that it has adjusted to a state where it no longer flows primarily offshore but rather propagates primarily along the isobaths. This depth needs to be distinguished from the (sometimes significantly greater) equilibrium depth corresponding to the point where the outflow’s density equals the environmental density.] Most of the time, the outflow descent is accompanied by a reduction in the bottom slope  $S$ , and an entrainment which causes both a reduction in  $g'$  and an increase in  $H$ . All of these alterations bring the outflow closer and closer to the critical condition and it is, therefore, argued that all outflows ultimately reach the critical point (unless diffusion and mixing destroy them prior to that stage).

It is suggested that Reddies (i.e., isolated lenses containing Red Sea water) are formed by the above processes. Namely, we propose that the “Reddy maker” is a combination of three processes, the natural reduction in the bottom slope which the outflow senses as it approaches the bottom of the ocean, the entrainment-induced increase in the outflow’s thickness, and the entrainment-induced decrease in the outflow’s density. An animation of the eddy generation process can be viewed at <http://doronnof.net/features.html#video> (click on “Reddy maker video”).

© 2002 Elsevier Science Ltd. All rights reserved.

\*Corresponding author. Fax: +1-850-644-2581.

E-mail addresses: nof@ocean.fsu.edu (D. Nof), paldor@vms.huji.ac.il (N. Paldor).

<sup>1</sup>Also affiliated with The Geophysical Fluid Dynamics Institute, Florida State University.

Nomenclature			
$f$	Coriolis parameter	$S_c$	critical slope
$g'$	“reduced gravity”	$u, v$	horizontal velocity components
$H$	maximum thickness	$\alpha$	coefficient of order unity (depends on the potential vorticity distribution)
$h$	thickness	$\beta$	variation of the Coriolis parameter with latitude
$P$	potential vorticity	$\gamma = b/R_d$	ratio between current width and the Rossby radius
$Q$	outflow’s discharge	$\delta$	vorticity coefficient of the eddies
$R$	eddies’ radius	$\mu$	angle of slope
$S$	bottom slope ( $\tan \mu$ )		

## 1. Introduction

Understanding the distribution of Reddies in the Indian Ocean is important to the determination of the general density structure in the ocean which, in turn, is an important aspect of the thermohaline circulation. Here, we focus on processes controlling the formation and distribution of these eddies. In particular, we shall address the issue of varying bottom topography and its effect on the Red Sea outflow. We shall argue that because of the very small density difference ( $\Delta\rho$ ) associated with Reddies ( $\Delta\rho/\rho \sim 10^{-5}$  compared to, say, the Mediterranean outflow where  $\Delta\rho/\rho$  is much greater, roughly  $10^{-3}$ ), a continuous Red Sea outflow cannot exist.

### 1.1. Observational background

Although there have not been any direct observations of Reddies, it has been argued on the basis of hydrographic data that Reddies are occasionally present off the horn of Africa (see Figs. 1 and 2, and Shapiro and Meschanov, 1991; Meschanov and Shapiro, 1998). They appear to be closely related to their Atlantic Ocean counterparts (Meddies, which are lenses of Mediterranean water formed from the Mediterranean outflow) but there are also two important differences between Meddies and Reddies. The first is that the relative density difference between Reddies and their environment is of the order of  $10^{-6}$  or  $10^{-5}$ , much smaller than that of Meddies which is  $10^{-3}$ . This is probably due to very strong mixing and

entrainment taking place immediately to the east of the Strait of Bab-el-Mandeb. The second difference between the two is that Meddies are formed from an outflow situated along an eastern boundary (and, hence, tend to spread westward into the interior of the ocean due to the variation of the Coriolis parameter with latitude,  $\beta$ ) whereas Reddies are formed from an outflow situated along a western boundary (and, hence, are less likely to spread into the entire Indian Ocean).

Because of the close relationship between Meddies and Reddies and because Meddies have been much more thoroughly documented than Reddies, it is useful to first review the behavior of Meddies. We begin by pointing out that Meddies are an integral part of the Mediterranean tongue (see Armi and Zenk, 1984; Richardson et al., 1989; see also Price et al., 1993; Spall et al., 1993; Prater and Sanford, 1994; Bower et al., 1995). They contain a mixture of Mediterranean and North Atlantic water (Armi and Zenk, 1984; McWilliams, 1985; Hebert et al., 1990), have a diameter of roughly 50–80 km and a thickness of  $\approx 1000$  m. They appear to move relative to their environment at speeds of a few centimeters per second (Richardson et al., 1989), and to persist for long periods of time (Armi et al., 1989).

The fate of some Meddies appears to be catastrophic interactions with seamounts (Richardson et al., 1989); however, there are indications that Meddies can cross the entire North Atlantic basin. Eddies with properties consistent with source regions near the Mediterranean have been observed in the site of the Local

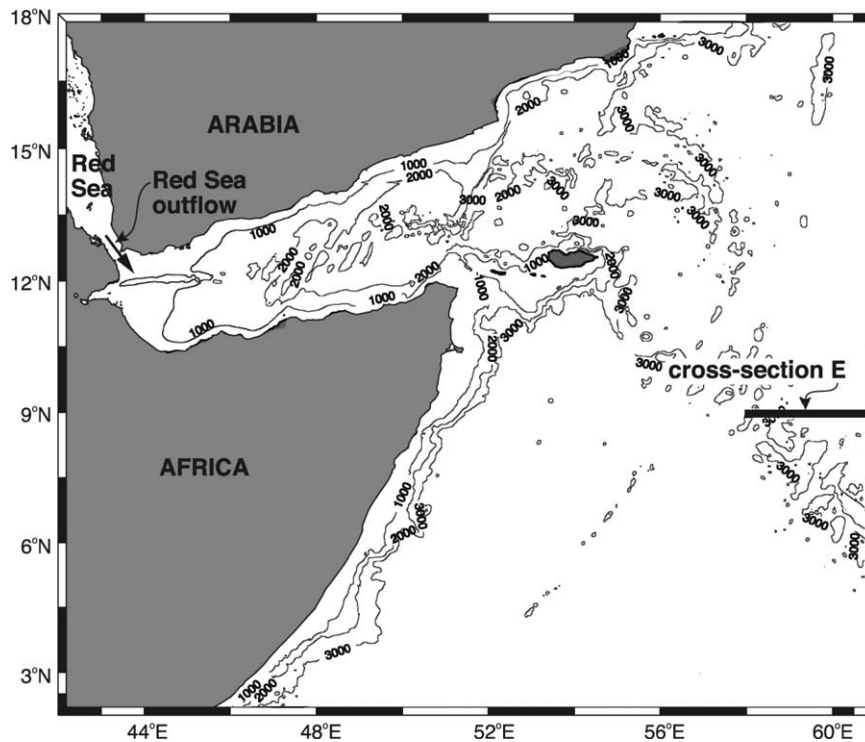


Fig. 1. Topography of the Gulf of Aden and the western Indian Ocean (provided by A. Bower). Depth contours are in meters. Section E is shown in Fig. 2.

Dynamics Experiment (LDE) and the Bahamas (Ebbesmeyer et al., 1986; McDowell and Rossby, 1978). The effect of Meddies on the North Atlantic structure is not currently clear. However, the LDE suggests that the general population of submesoscale coherent vortices (SCVs) in the North Atlantic is enormous (Ebbesmeyer et al., 1986) supporting the suggestion of Armi and Zenk (1984) that Meddies constitute a principal mechanism for the spread of Mediterranean water.

Like Meddies, Reddies are a few hundred meters thick and have a diameter of 100–200 km (Meschanov and Shapiro, 1998). In the Gulf of Aden Red Sea water is found at depths of 400–700 m but it sinks to 600–900 m as it moves eastward to the Arabian Sea. Although the Mediterranean outflow mass flux ( $\approx 1 \text{ Sv}$ ) is greater than the Red Sea outflow mass flux ( $\approx 0.2 \text{ Sv}$ ) and although  $\beta$  tends to increase the spreading of the Mediterranean outflow and suppress the spreading of the Red Sea

outflow, the effect of Reddies on the ocean is expected to be quite important because the density flux (mass flux times the density anomaly) is still large compared to that of other ocean currents. The reader is referred to Bower et al. (2000) for related aspects of the Red Sea outflow.

### 1.2. Theoretical background

Like Meddies, Reddies belong to the so-called SCVs category because their length scale is smaller than the surrounding Rossby radius; their scale is, however, of the order of the Rossby radius based on *their own* vertical structure. SCVs received much attention (see e.g., the review articles of McWilliams, 1985; Flierl, 1987) but most of this attention focused on their stability and propagation on a  $\beta$  plane. Why and how Meddies and Reddies are generated in the first place is still not entirely clear. Traditionally, their formation

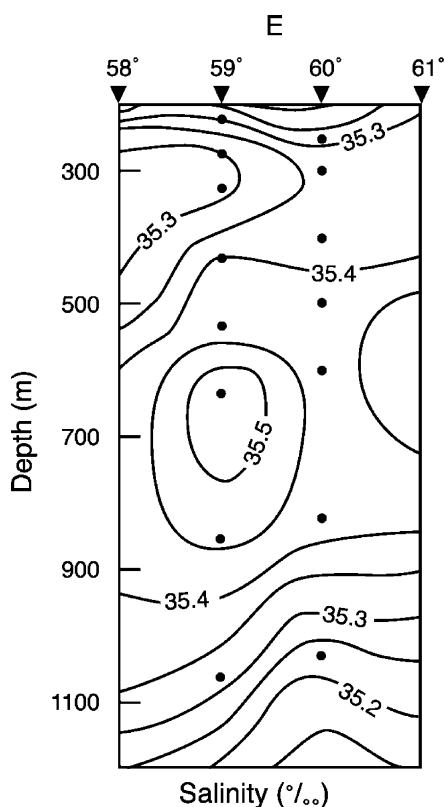


Fig. 2. Hydrographic sections of salinity (‰) along 9°N through a typical Reddy [lens 5 (May 1979)]. Dots represent data points. Triangles at the top indicate the location of the hydrographic stations. Adapted from Shapiro and Meschanov (1991). The location of Section E is shown in Fig. 1.

process was associated with the instability of frontal currents (Shapiro and Meschanov, 1991; Käse et al., 1989; see also Stern, 1980; Stern et al., 1982; Griffiths and Linden, 1981, 1982; Griffiths et al., 1982; Griffiths and Hopfinger, 1983; Griffiths, 1986). McWilliams (1988) suggested that mixing over continental shelves followed by geostrophic adjustment may be responsible for the formation of Meddies. Nof (1991), on the other hand, suggested that intermittencies in the outflow can produce discrete eddies even if the currents were otherwise stable and remain attached to the boundary.

Many of the Meddies seem to be generated in the same general area suggesting a topographical

or geographical influence. An explanation consistent with this observation has been suggested by D'Asaro (1988) who, on the basis of vorticity arguments, concluded that boundary currents that detach from the coast must somehow produce rings. He did not investigate, however, how and why the eddies are generated. A similar process associated with time-dependent separation of a coastal current was examined by Stern and Whitehead (1990), but, again, it is not obvious that time-dependent inflow is crucial for the actual general process in the ocean. Studies have also been made of steady or quasi-steady eddies generated at a corner (e.g., Cherniawsky and LeBlond, 1986; Klinger, 1994a, b). Alternative formation mechanisms related to instabilities are discussed by Griffiths et al. (1982), Condie (1995), Baines and Condie (1998), Spall and Price (1998), Swaters (1991), Whitehead et al. (1990), and Lane-Serff and Baines (1998). The work of Røed (1980) and Klinger (1994a) imply that inconsistency between the upstream and downstream conditions can lead to a breakup of the flow. Recently, Pichevin and Nof (1997) have suggested that a combination of zonal capes,  $\beta$  and advection are responsible for the formation of Meddies. Since we are dealing here with an outflow along a western boundary rather than eastern,  $\beta$  cannot be the agent responsible for Reddy formation. It is for this reason that we consider here a (bottom) topography-induced eddy-generation mechanism and argue that a mechanism different from that which produces Meddies is probably responsible for the formation of Reddies.

To show that bottom topography might be the agent responsible for Reddy formation, we first address the dynamics of a continuous inviscid outflow situated over a gradually varying slope (Section 2). This is followed by a derivation of the analytical constraints which lead to the establishment of the minimum (or critical) slope criteria. Namely, we show analytically (in Section 3) that, in order for the outflow to exist as a continuous uninterrupted slowly varying current, the bottom slope must be supercritical, i.e., greater than a critical slope. We shall also show that when the bottom slope is subcritical (i.e., smaller than the critical slope), the

outflow can only consist as a chain of propagating eddies.

We shall see that the criticality condition results from the following combination of circumstances. Since there is only one upstream source of anomalous water, it is clear that the velocity of the continuous outflow must be positive at all points across the outflow, i.e., there is no anomalous water coming from infinity. This condition of positive velocity everywhere appears to be one which would be easily satisfied but it turns out that this is not at all the case. To see this, we shall first note that the speed of the fluid within the outflow can be thought of as a super-position of two independent velocity profiles, one velocity profile is that of the outflow as if it were situated on a flat bottom and the other is the slope-induced advection. The former is always associated with both negative and positive speeds as the interface bounding the outflow from above must change its slope from positive to negative across the outflow; this results in positive flow on the left-hand side (looking downstream) and negative flow on the right-hand side. The latter velocity profile, on the other hand, is always positive. These imply that the absolute velocity (i.e., the sum of the two) will be positive everywhere only when the slope-induced advection is greater than the negative velocity associated with the (hypothetical) outflow over a flat bottom. Namely, the slope-induced speed must be greater than a threshold value which is determined by the slope and the intensity of the outflow.

When the slope-induced speed does not exceed the threshold value the outflow must have negative speeds somewhere and this is a physically realizable situation only when it consists of a chain of isolated lenses. Negative velocities are allowed in this eddy case because here they do not correspond to anomalous water originating at infinity but rather to *locally* circulating fluid.

In Section 4 we present nonlinear reduced-gravity numerical simulations which clearly support the analytical conclusions. In this context, we make a clear distinction between the classical instability mechanism leading to eddy formation via the breakdown of a known steady solution (e.g., Griffiths et al., 1982) and our new eddy-

maker mechanism which corresponds to a situation where a *steady solution cannot exist*. The results are summarized and the application to the Red Sea outflow is discussed in detail in Section 5.

## 2. Formulation

Consider the situation shown in Fig. 3. An inviscid dense outflow (whose density is  $\rho$ ) is flowing along the isobaths of a bottom whose slope is uniform in the cross-isobaths direction ( $y$ ) but varies (gradually) in the long-isobaths direction ( $x$ ). The infinitely deep fluid above the outflow has a density ( $\rho - \Delta\rho$ ) and is taken to be at rest. The governing equations for a steady frictionless Boussinesq fluid are,

$$u \frac{\partial u}{\partial x} + v \frac{\partial u}{\partial y} + f \left( v + \frac{g' y \partial S / \partial x}{f} \right) = g' \frac{\partial h}{\partial x}, \quad (2.1)$$

$$u \frac{\partial v}{\partial x} + v \frac{\partial v}{\partial y} + f \left( u \frac{g' S}{f} \right) = g' \frac{\partial h}{\partial y}, \quad (2.2)$$

$$\frac{\partial(hu)}{\partial x} + \frac{\partial(hw)}{\partial y} = 0, \quad (2.3)$$

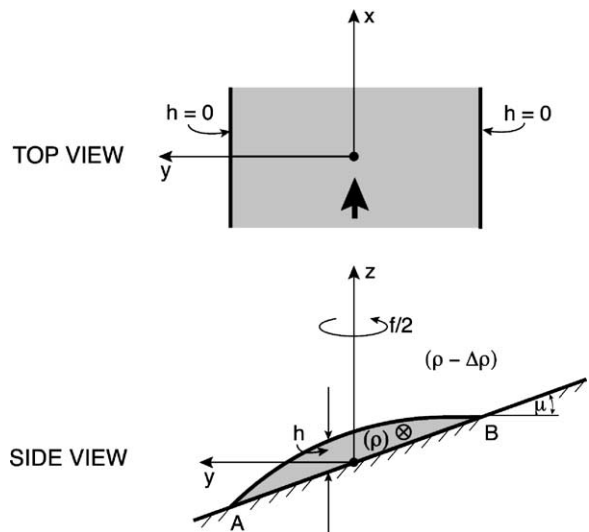


Fig. 3. Schematic diagram of the dense outflow under study. The nonlinear inviscid outflow is progressing along the isobaths of a bottom whose uniform slope  $S (= \tan \mu)$  varies gradually in  $x$  (i.e., the long-stream direction) but not in  $y$ , i.e.,  $S = S(x)$ .

where the deviation of the hydrostatic pressure from the hydrostatic pressure associated with a state of rest (i.e., no outflow) is

$$P(z) = g \Delta\rho[h - S(x)y + z], \tag{2.4}$$

with  $S(x) = \tan(\mu(x)) \ll 1$  and  $g' = g\Delta\rho/\rho$ . Our conventional notation is defined both in the text and in the Nomenclature. Namely,  $u$  and  $v$  are the horizontal velocity components,  $f$  is the Coriolis parameter,  $g$  the acceleration of gravity, and  $h$  is the thickness.

It is apparent that, in the case of a continuous outflow overlaying a bottom slope that is varying slowly in  $x$ , the last term on the left-hand side of (2.1) can be neglected. Note, however, that this is not the case for an outflow that consists of a chain of eddies because in that case the flow length scale in the  $x$  direction is the same as that along the  $y$  direction. We shall return to this important point later. Under such conditions (i.e., a flow with a topography corresponding to a small  $\partial S/\partial x$ ), the contribution of the bottom slope enters the problem only through the last term on the right-hand side of (2.2) which is linear. As pointed out by Griffiths et al. (1982), this implies that the problem can be decomposed into two components (Fig. 4). The first is a two-directional outflow on a flat bottom (Fig. 4, upper panel) and the second is a topography-induced advection (Fig. 4, lower

panel). We shall shortly see that this decomposition is of crucial importance to our analysis.

### 3. Analytical constraints

#### 3.1. An outflow or a chain of eddies?

As mentioned, for an outflow of the kind shown in Fig. 3 to exist it is, of course, necessary that the long-isobaths velocity be positive everywhere as there is only one (upstream) source of dense water. In view of the decomposition mentioned earlier, this condition implies that a continuous outflow can exist only if

$$\frac{g'S}{f} > |u_B|, \tag{3.1}$$

where  $u_B$  is the negative velocity of the outflow on a flat bottom at point B (Fig. 3). For a zero potential vorticity outflow (i.e.,  $-\partial u/\partial y + f = 0$ ), the velocity profile is linear ( $u = fy$ ) and (by cross-stream geostrophy) the thickness profile is found to be

$$h = H \left( 1 - \frac{y^2}{2R_d^2} \right), \tag{3.2}$$

where  $R_d^2 = g'H/f^2$  and  $H$  is the maximum thickness. Relation (3.2) implies that the outflow's

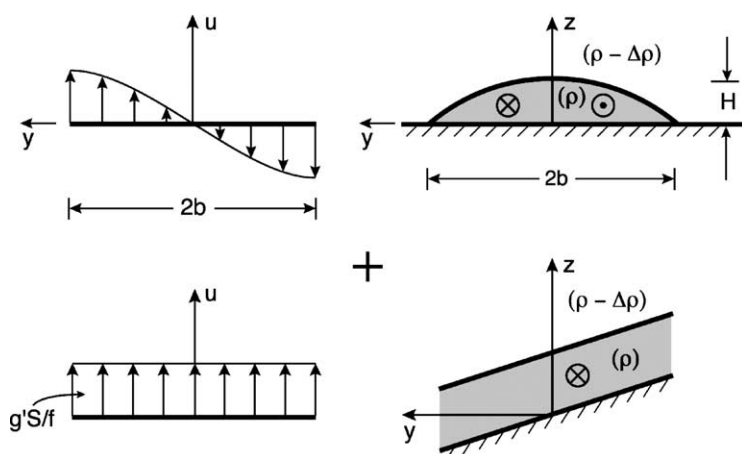


Fig. 4. The decomposition of the outflow (shown in Fig. 3) into two components, an outflow on a flat bottom (upper panels) and a uniform topography-induced advection (lower panels). The panels on the left show the velocity profiles and the panels on the right show cross-sections of the decomposed outflow.

half-width is  $\sqrt{2}R_d$  which means that the speed along point B (shown in Fig. 3) is  $u_B = (2g'H)^{1/2}$ . In view of this, (3.1) gives,

$$\frac{g'S}{f} \geq (2g'H)^{1/2}, \quad (3.3)$$

as the necessary condition for the existence of a continuous zero potential vorticity outflow.

This condition must, of course, hold along the entire path of the outflow. When (3.3) is not satisfied, the (single) outflow contains negative velocities (on the uphill side) which imply a flow coming from infinity. We reject this kind of an outflow as “unphysical” as our system contains a single (upstream) source of water. We shall argue that, under these conditions, the outflow can only exist as a chain of propagating eddies because eddies can have negative velocities which do not correspond to water coming from infinity. This is so because negative velocities on the uphill side of the eddies correspond simply to locally circulating fluid.

When the potential vorticity  $P$  is uniform but not zero, i.e.,  $P = f/H$  (where  $H$  is again the maximum thickness [and  $b \gg R_d$  (i.e., the outflow is broad)], both the  $u$  velocity component and the thickness have an exponential profile,

$$\begin{aligned} h &= H \left[ 1 - \frac{\gamma}{(\gamma^2 + 1)} (e^{y/R_d} + e^{-y/R_d}) \right], \\ u &= (g'H)^{1/2} \left[ \frac{\gamma}{(\gamma^2 + 1)} (e^{y/R_d} - e^{-y/R_d}) \right], \end{aligned} \quad (3.4)$$

where  $\gamma = e^{b/R_d}$ . When  $y \rightarrow -b$  and  $b \gg R_d$ ,  $u$  goes to minus  $(g'H)^{1/2}$ . Consequently, for our present uniform potential vorticity case, the positive velocity everywhere condition (3.3) is modified to,

$$\frac{g'S}{f} \geq (g'H)^{1/2}, \quad (3.5)$$

implying that, in the most general form (i.e., nonuniform and nonzero potential vorticity), the condition can be written as

$$\frac{g's}{f} \geq (g'H)^{1/2}, \quad (3.6)$$

Accordingly, we define the critical slope  $S_c$  to be,

$$S_c \geq \frac{\alpha f (g'H)^{1/2}}{g'}, \quad (3.6a)$$

where  $\alpha$  is a coefficient of order unity which depends on the outflow's potential vorticity distribution. As mentioned, when the above condition is not met the outflow cannot exist as a continuous current because it cannot have water originating at infinity where there are no sources. It is expected that, under such conditions, the outflow will exist as a chain of anticyclonic eddies propagating along the topography. Again, as mentioned, this is so because such propagating eddies can have negative velocities on their uphill side and yet carry mass forward. Namely, since such eddies are in fact isolated lenses (i.e., they are bounded by a closed contour corresponding to  $h = 0$ ) a negative velocity on the uphill side does not represent fluid coming from infinity but rather a *locally* circulating fluid.

Using a numerical simulation of a dense outflow overlying a slope that decreases gradually in  $x$ , we shall shortly show (Section 4) that the above is indeed the case. Namely, we shall show that an outflow which is initially situated over a supercritical slope satisfying (3.6) is continuous but is converted into a chain of eddies once it enters a region where the condition is not satisfied, i.e., when the slope is subcritical.

### 3.2. The eddies' size

We shall now determine the expected size of zero and nonuniform potential vorticity eddies resulting from outflows on a subcritical slope ( $S < S_c$ ). Assuming that the eddies (resulting from a zero potential vorticity outflow) are osculating each other as they drift along the isobaths, their radius  $R$  is immediately found to be

$$R = \left( \frac{32Q}{\pi S f} \right)^{1/3}, \quad S < S_c, \quad (3.7)$$

where  $Q$  is the outflow's discharge. For an outflow of 0.3 Sv, a slope of 0.02 and an  $f$  of  $10^{-5} \text{ s}^{-1}$ , the radius is 25 km. In deriving (3.7) it has been taken into account that the volume of each individual zero potential vorticity eddy is  $\pi f^2 R^4 / 16g'$  and

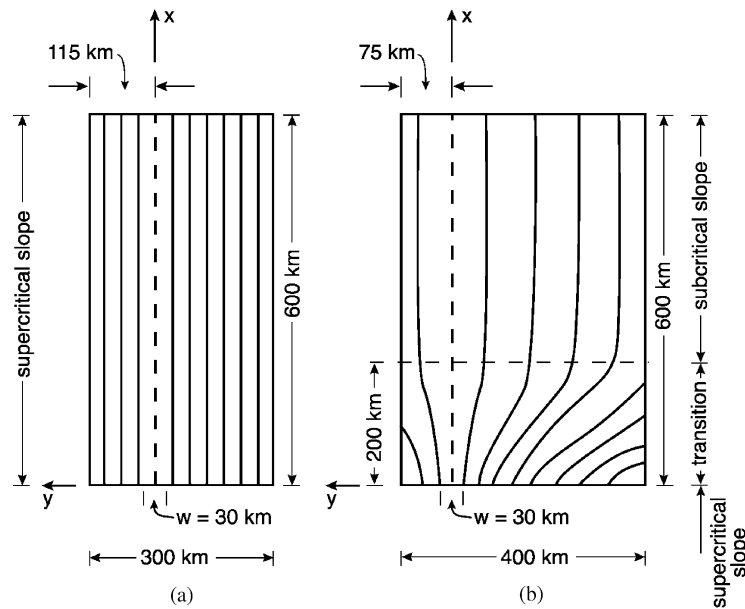


Fig. 5. The isobaths for the constant [panel (a)] and variable [panel (b)] slope experiments. For all runs the inflow was specified at the lower boundary and had a width  $w$  of 30 km. The inflow axis (dashed line) was located on a straight isobath so parcels that remain along the axis do not flow uphill or downhill. Orlandi radiation conditions were applied at the left, right and downstream boundaries. Constant slope runs (left) had a basin size of 300 km  $\times$  600 km with the inflow axis located 115 km from the left boundary. Variable slope runs (right) had a slightly wider basin of 400 km  $\times$  600 km. The inflow axis was located 75 km from the left boundary for runs with an upstream slope = 0.03 and 95 km from the boundary for runs with an upstream slope = 0.02 or 0.016. The slope decreased smoothly from its upstream value ( $S_0$ ) at  $x = 0$  to its downstream value ( $S_2$ ) at  $x = 200$  km. Specifically, the topography is given by  $H(x, y) = H(0) - S(x)y$  where  $S(x)$  is a cubic function that varies from  $S_0$  at  $x = 0$  to  $S = S_1$  at  $x = 200$  km with  $\partial S/\partial x = 0$  at  $x = 0, 200$  km.

that it drifts along the isobaths at  $g'S/f$  (Nof, 1983). The corresponding periodicity is found from the drift speed to be  $2R/g'S/f$ .

Since there is no known analytical solution for a uniform potential vorticity eddy,<sup>2</sup> the analogous expression of (3.7) for a uniform potential vorticity eddy cannot be derived. We may, however, consider eddies with a linear orbital velocity ( $v_\theta$ ) profile,

$$v_\theta = -\frac{\delta}{2}fr,$$

where  $\delta$  is the vorticity coefficient of the eddies, is smaller than unity. Such eddies correspond, of course, to nonuniform potential vorticity. The volume of each of these eddies is

<sup>2</sup>Csanady (1979) derived an approximate solution for a uniform potential vorticity eddy but Flierl (1979) has shown that the solution breaks down along the edge.

$\delta(2 - \delta)\pi f^2 R^4/16g'$  implying that their radius is

$$R = \left[ \frac{32Q}{\alpha(2 - \delta)\pi Sf} \right]^{1/3}. \tag{3.8}$$

Since the potential vorticity of these eddies is not uniform, it is difficult to compare them to our numerical runs. We chose, nevertheless, to present the above results as they provide a more complete picture. We shall see in the next section that even though the initial zero potential vorticity of the outflow is altered as the eddies are formed (the relative vorticity decreases from  $-f$  to  $-f/2$ ), (3.7) is in good agreement with the numerics.

#### 4. Numerical simulations

To analyze the validity of the above calculations, we shall now present numerical simulations

Table 1  
Details of the experiments

Exp.	Description	Slope	Upstream slope	Downstream slope	Downstream subcritical? ( $S < S_c$ )	Upstream vorticity	Transport (Sv)	Lateral viscosity ( $\text{m}^2 \text{s}^{-1}$ )	Result	Shown in Figs.
1		Constant	0.03	0.03	No	$-f$	0.675	20	Straight w/strong waves	
2		Constant	0.03	0.03	No	$-f$	0.675	30	Straight w/strong waves	
3	Fig. 5a	Constant	0.03	0.03	No	$-f$	0.675	40	Straight w/weak waves	
4		Constant	0.03	0.03	No	$-f$	0.675	70	Straight w/weak waves	
5		Constant	0.03	0.03	No	$-f$	0.675	100	Straight w/weak waves	
6		Constant	0.03	0.03	No	$-f$	0.675	200	Straight	
7	Fig. 5b	Variable	0.03	0.003	Yes	$-f$	0.675	20	Eddies	7 and 8
8		Variable	0.03	0.003	Yes	$-f$	0.675	30	Eddies	7 and 8
9		Variable	0.03	0.003	Yes	$-f$	0.675	40	Eddies	7 and 8
10		Constant	0.02	0.02	No	$-f$	0.450	5	Straight w/strong waves	
11	Fig. 5a	Constant	0.02	0.02	No	$-f$	0.450	10	Straight w/strong waves	
12		Constant	0.02	0.02	No	$-f$	0.450	20	Straight w/weak waves	
13		Constant	0.02	0.02	No	$-f$	0.450	45	Straight	
14	Fig. 6b left	Variable	0.02	0.003	Yes	$-f$	0.450	5	Eddies	6b, 7 and 8
15	Fig. 6a right	Variable	0.02	0.003	Yes	$-f$	0.450	10	Eddies	6a, 7 and 8
16		Constant	0.016	0.016	No	$-f$	0.360	5	Straight w/strong waves	
17	Fig. 6a left	Constant	0.016	0.016	No	$-f$	0.360	10	Straight	6a
18		Constant	0.016	0.016	No	$-f$	0.360	40	Straight	
19	Fig. 6a right	Variable	0.016	0.003	Yes	$-f$	0.360	5	Eddies	6b, 7, 8 and 9
20	Fig. 6b right	Variable	0.03	0.003	Yes	$-0.323 f$	0.218	3	Eddies	6c
21	Fig. 5b	Variable	0.03	0.025	No	$-f$	0.675	30	Straight w/weak waves	6d
22	Fig. 5b	Variable	0.02	0.003 & 0.02	Yes and no	$-f$	0.450	10	Eddies/straight in supercritical/subcritical region	6e

Note: For all experiments we chose  $f = 1 \times 10^{-5} \text{ s}^{-1}$ ,  $g' = 9.8 \times 10^{-5} \text{ m s}^{-2}$ , and an inflow width ( $w$ ) of 30 km. The Rossby radius ( $R_d$ ), based on the central depth of the inflow ( $H_{\text{max}} = 115 \text{ m}$ ) was 11 km. The critical slope (based on the condition of zero speed at the right-hand front of the inflow) was 0.015. The spatial grid size was 2 km and the time step 240 s. For constant slope runs the domain was 300 km  $\times$  600 km (Fig. 5a) and for the variable slope runs it was a slightly wider 400 km  $\times$  600 km (Fig. 5b). The slope varied smoothly from its upstream value at  $x = 0$ , to its downstream value at  $x = 200 \text{ km}$ . For  $x$  greater than 200 km, the slope did not vary.

of an outflow overlaying a gradually varying slope and quantitatively analyze the results.

#### 4.1. Numerical model description

We used the Bleck and Boudra (1986) reduced gravity isopycnic model with a passive upper layer and employed the Orlanski (1976) second-order radiation condition for the open boundary. We found that this condition is satisfactory because the downstream streamlines were not disturbed when they crossed the boundary. In order to verify that the simulated eddies are indeed generated by the subcritical slope rather than by the familiar instability of double frontal currents (e.g., Griffiths et al., 1982), we performed both uniform supercritical slope experiments and variable slope experiments. Before concluding that the eddies were generated by the very small ( $S < S_c$ ) slope we verified that the identical outflow remains coherent on a steeper slope ( $S > S_c$ ), i.e., that the outflow is *stable*. The uniform and varying topography that we used is shown in Fig. 5. We performed a total of twenty experiments with varying slopes and viscosity (Table 1).

All runs were conducted with a relatively high resolution corresponding to  $\Delta x = \Delta y = 2$  km. For numerical stability, we chose an eddy viscosity of  $5\text{--}200\text{ m}^2\text{ s}^{-1}$ ; the time step was 240 s and the

maximum thickness was 115 m. These choices are certainly adequate for a Rossby radius of 11 km (corresponding to a  $g'$  of  $9.8 \times 10^{-5}\text{ m s}^{-2}$  and  $f_0 = 10^{-5}\text{ s}^{-1}$ ). Furthermore, these choices always allowed for at least ten grid points across the downstream current, which is also adequate. Our mass flux was about one-half Sv and we used an inflow 30 km wide.

The inflow's potential vorticity was zero in most of these runs (all but Exp. 20) but the friction (required for numerical stability) was large enough to reduce the relative vorticity from an initial value of  $-f$  to  $-f/2$  (by the time that the first eddy was formed). This means that the runs really correspond to a constantly modified nonuniform potential vorticity (as is the case in the real ocean). To examine the sensitivity of our runs to the inflow conditions we also conducted a run (Exp. 20) with an upstream relative vorticity of  $-0.323f$ . As we shall see, the results are very similar to those of the zero potential vorticity inflow.

#### 4.2. Results

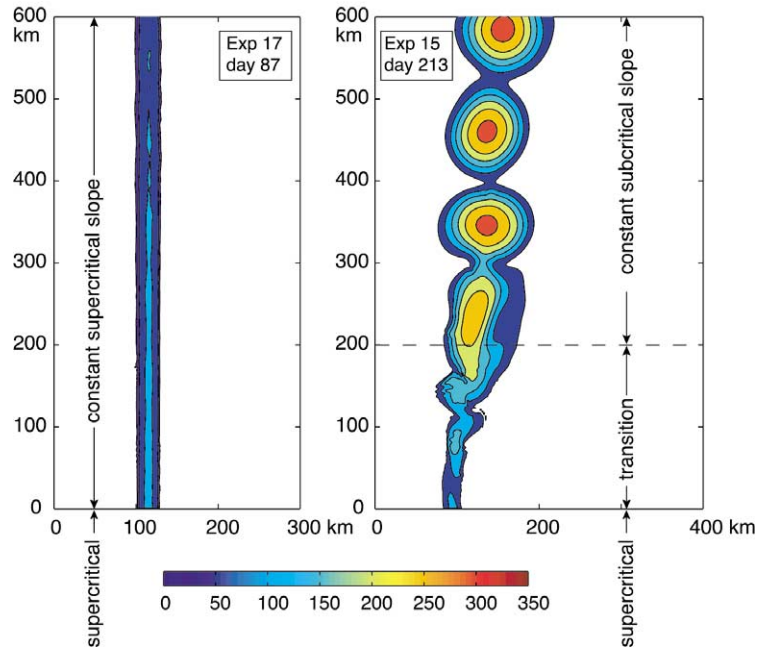
The results are shown in Figs. 6–9, all of which display a good agreement with the theory. Figs. 6a–c all show that, as the theory predicts, a chain of eddies is indeed established when the bottom slope becomes subcritical ( $S < S_c$ ). When



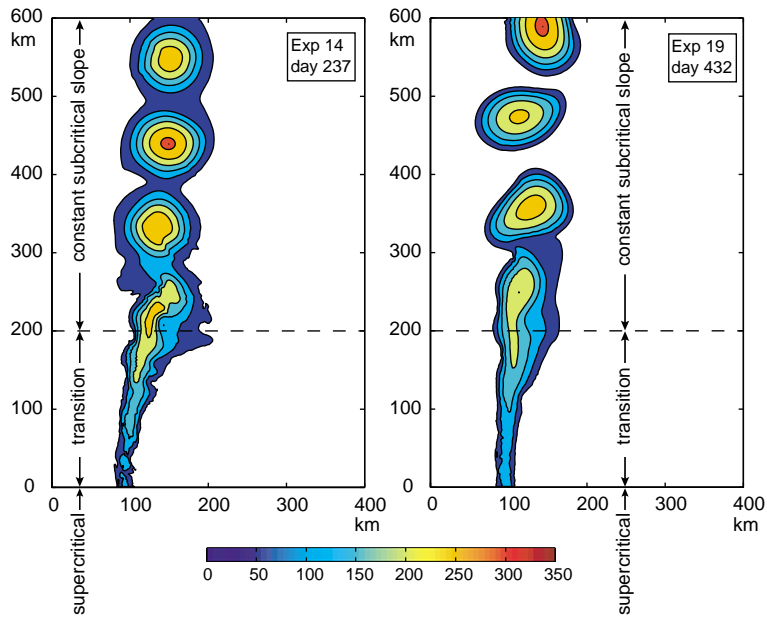
Fig. 6. (a) Snapshots of the thickness field for a “typical” reference simulation with a constant supercritical slope (Exp. 17, left panel) and a comparable simulation with a variable slope (Exp. 15, right panel). In both experiments the inflow width is 30 km and  $v = 10\text{ m}^2\text{ s}^{-1}$  indicating that the relative importance of frictional forces ( $v/fL^2$ ) is the same in both experiments. For the experiments described by the left panel the slope had a constant supercritical value, 0.02, everywhere, while for the experiment described in the right panel the slope changed smoothly from the supercritical value 0.016 for  $x \leq 0$  to the subcritical value 0.003 for  $x \geq 200$  km. In the constant slope experiment (left panel) the inflow remained steady and straight with no signs of breaking into eddies, i.e., the double frontal current is stable. But as the steady jet flowed over a variable slope  $0 \leq x \leq 200$  km (right panel) and entered a subcritical region, it turned into a chain of propagating eddies with a mean radius and periodicity of 60 km and 49 days, respectively. Both values are within 17% of the theoretical values of 53 km and 42 days (see Figs. 7 and 8). (b) Snapshots of the thickness field for additional “typical” experiments [Exp. 14 (left panel) and Exp. 19 (right panel)]. As in Fig. 6a, the inflow width was 30 km but now  $v = 5\text{ m}^2\text{ s}^{-1}$ . In both experiments the slope was variable, changing in the left panel from the supercritical value 0.02 for  $x \leq 0$  to the subcritical value 0.003 for  $x \geq 200$  km, and in the right panel from 0.016 for  $x \leq 0$  to 0.003 for  $x \geq 200$  km. In Exp. 14, the bottom slope changed more severely than the bottom in Exp. 19 and, hence, the flow was less organized. (c) Snapshot of the thickness field for Exp. 20 (the nonzero potential vorticity experiment). As in Fig. 6b, the inflow width is 30 km and the slope is variable (in this case changing from the “supercritical” value of 0.03 for  $x \leq 0$  to the “subcritical” value 0.003 for  $x \geq 200$  km) but now the upstream relative vorticity is  $-0.323f$  rather than  $f$ . Note that we used “supercritical” and “subcritical” in quotation marks because in the nonuniform potential vorticity case discussed here it only applies to the incoming flow. The critical slope for our specified inflow (upstream) shear is 0.015. Physical parameters:  $\delta = 0.323$ ,  $v = 3\text{ m}^2\text{ s}^{-1}$  and  $\Delta\rho/\rho = 0.323 \times 10^{-5}$ . (d) The same as the right panel of Fig. 6a except that the slope returns to the original slope downstream. Note that the eddies merge and form a current similar to the incoming flow. (e) The same as Fig. 6a except that it has a higher upstream slope and that the slope never reaches a subcritical value. Consequently, eddies do not form.

the bottom slope was supercritical (e.g., Fig. 6a left panel) the outflow *remained coherent* indicating that the slope-induced eddy-generation mechanism is not related to the instability of a double frontal

current, i.e., it is not associated with the breakdown of a known steady solution as this solution remained unaltered during the course of the simulation.



(a)



(b)

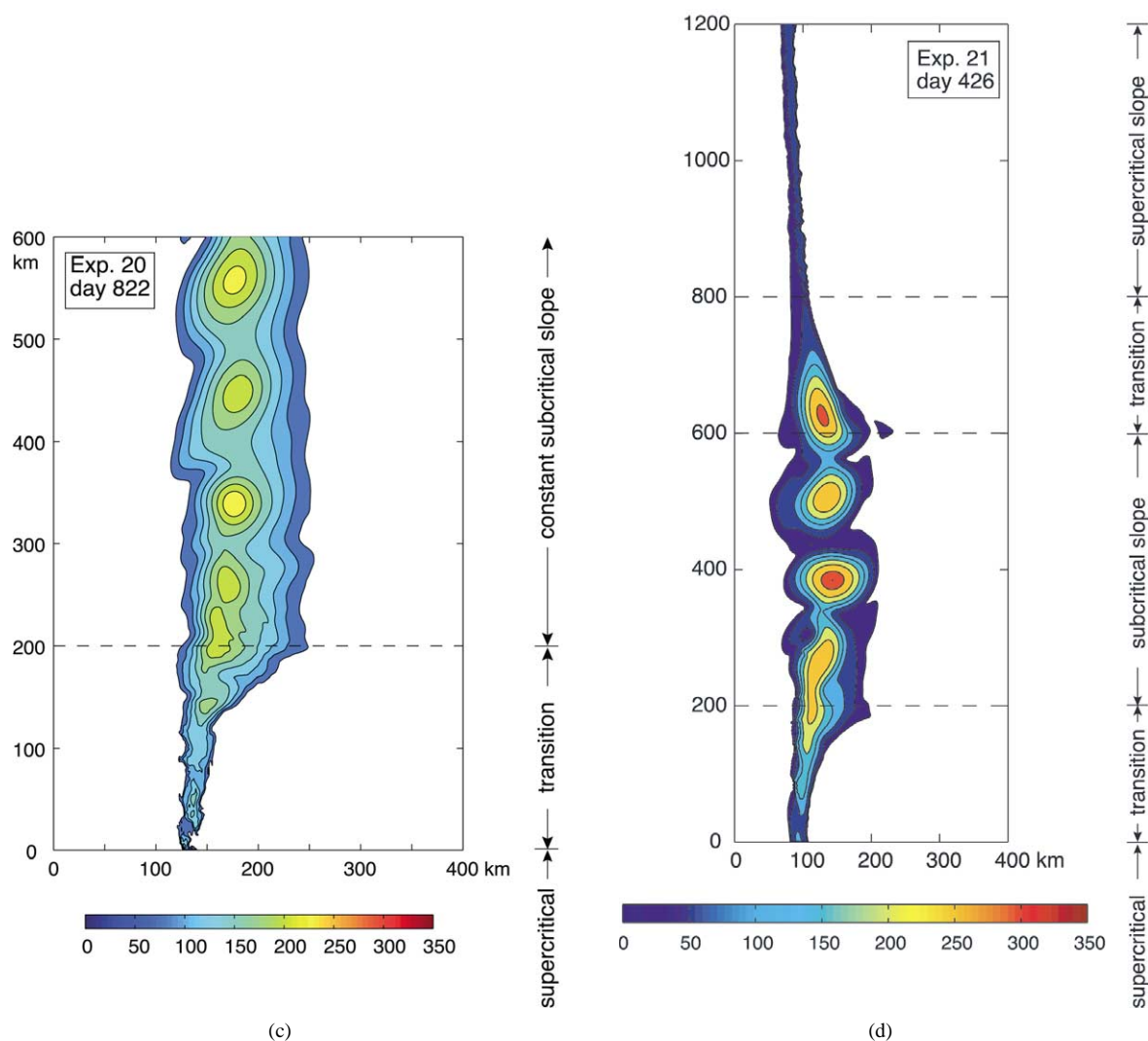
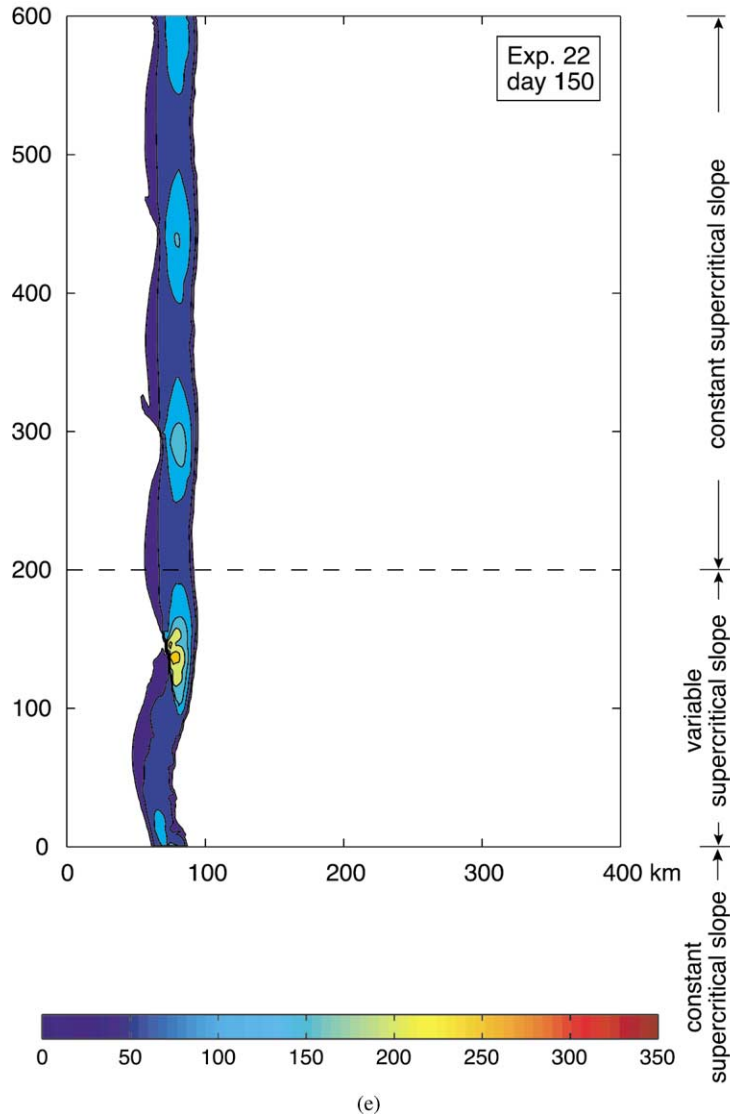


Fig. 6 (continued).

In the left panel of Fig. 6b (Exp. 14) we show an experiment identical to that of the right panel of Fig. 6a (Exp. 15) except that the viscosity is half of what it was before. The differences between the two are minute and insignificant, showing that lateral viscosity does not play a crucial role in the dynamics. In the right panel of Fig. 6b (Exp. 19) we show an experiment identical to that of the left panel of Fig. 6a (Exp. 17) except that the slope varies in the field and becomes subcritical. This variation causes the establishment of eddies and is the main point of this work. In Fig. 6c we show an

experiment (Exp. 20) with varying slope and nonzero potential vorticity. It shows that the main results (i.e., the breakup into eddies) are not very sensitive to the distribution of potential vorticity. In Fig. 6d we show an experiment (Exp. 21) where downstream the slope returns to the original supercritical upstream slope. [In all other respects the experiment is the same as that shown on the right panel of Fig. 6a (Exp. 15)]. We see that the eddies merge downstream and that a symmetrical structure is created. In Fig. 6e (Exp. 22) we show that eddies do not form when the slope changes



(e)  
Fig. 6 (continued).

but does not reach a subcritical value. Throughout the analytical–numerical comparison we varied the lateral viscosity dramatically to verify that it does not play a crucial role in the dynamics.

Figs. 7 and 8 show a comparison of the analytically predicted eddy periodicity and radius (based on the structure of zero potential vorticity eddies and on the assumption that the eddies are osculating each other as they propagate). We see that, as expected, the analytical solution provides a

lower bound on both the periodicity and the size. This is so because the numerical eddies have a lower vorticity than  $-f$  so that they are larger than those corresponding to zero potential vorticity.

All outflows show a tendency to veer slightly to the right from their upstream position (Fig. 6). This is due to the particular bottom topography that we chose. As shown in Fig. 5, the chosen sloping bottom “pivots” around the  $x$  axis. This implies that a particle moving in the positive  $x$

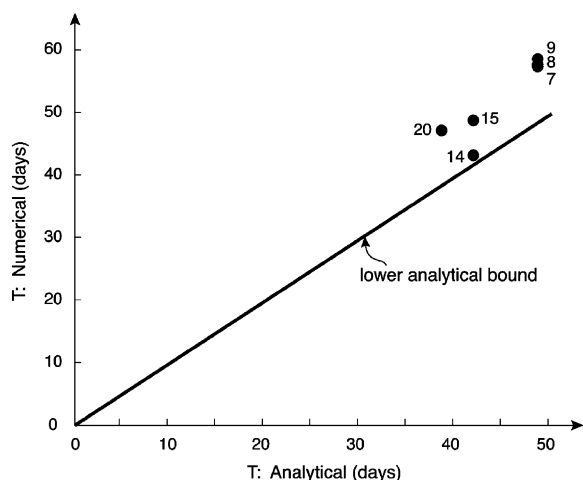


Fig. 7. Plot of the mean periodicity for each experiment as a function of its theoretical value, assuming that the eddies are osculating each other as they drift along the isobaths. The theoretical periodicity is plotted as a solid line. The simulated periodicity was measured by calculating the mean of the time intervals between successive maxima in the transport through a horizontal section at  $x=580$  km, just before the eddies exited the domain. The transport was lightly filtered to remove high frequency noise and the resulting maxima were checked to make sure they corresponded to the passing of an eddy. Numerals indicate the number of the experiment.

direction (at a constant  $y$ ) will sense an uphill movement to the left of the  $x$  axis (i.e.,  $y > 0$ ) and a downhill movement to the right of the  $x$  axis (i.e.,  $y < 0$ ). Since frictional forces induce a slight energy loss, the outflow is (very gradually) losing height and can only do so by veering to the right of its upstream path. Fig. 9 shows that, as already mentioned, the relative vorticity decreases significantly with friction (even though we chose relatively small frictional coefficients). On the other hand, the energy is nearly conserved during the experiments (Fig. 10) (though there is a conversion of kinetic to potential energy). The dramatic change in vorticity and the lack of such a dramatic change in the energy is consistent with the results obtained earlier by Borisov and Nof (1998) and Nof and Borisov (1998) where a current that broke up into eddies exhibited an order one change in the potential vorticity and virtually no change in the total energy. It is not at all obvious why there is such a difference between the effect of

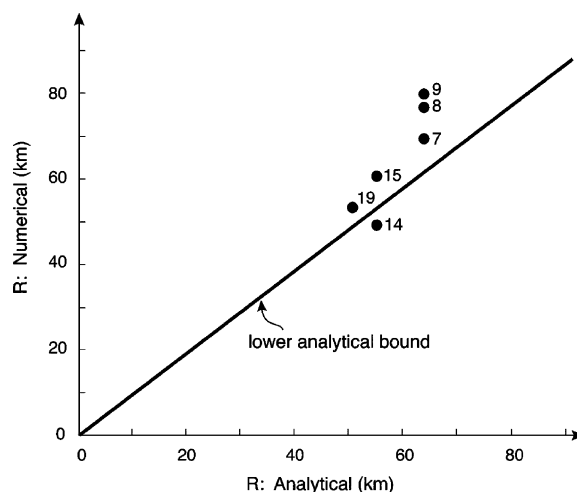


Fig. 8. As in Fig. 7, but for the mean eddy radius (for each experiment) as a function of its theoretical value, assuming again that the eddies are osculating each other as they propagate along the isobaths. The theoretical periodicity is plotted as a solid line. The radius of each numerical eddy was measured at a time just prior to its coming into contact with the downstream boundary of the domain. At that point in time, we measured the area enclosed by the depth contour at 50% of the central maximum depth. When the 50% contour was not closed, we measured the area inside the first closed contour. The radius of the eddy was then extrapolated according to  $r = [A/\pi(1 - \gamma)]^{1/2}$  where  $\gamma$  is the ratio of the depth of the contour enclosing the area  $A$  to the depth of the central maximum. As before, numerals indicate the number of the experiment.

friction on the vorticity and the energy. However, it probably stems from the fact that the alteration of vorticity merely requires broadening and spreading of the flow whereas changes in energy require more fundamental alterations, i.e., in our case, it is much easier for the fluid to change its vorticity than it is to change its energy.

## 5. Summary and discussion

The results of the theory can be summarized as follows:

1. Simple considerations related to the nonlinear dynamics of an inviscid double frontal current on a uniform slope (Figs. 3 and 4) show that, in order for such a current to exist as a continuous

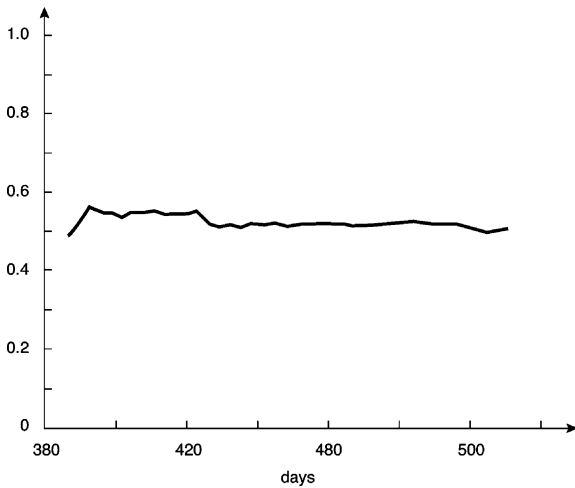


Fig. 9. Time evolution of the relative vorticity  $\xi$  in the core of a typical eddy (the eighth eddy generated in Exp. 19). The vorticity is scaled with its initial value,  $\xi(0) = -f$ . The plot starts on day 387 of the run, the first time at which eddy eight is recognizable.  $\xi/\xi(0)$  starts with the initial value of 1, because the fluid enters the domain as a zero PV jet. It is very difficult to trace particles as they travel from the inflow to the point where the stream changes into recognizable eddies, but by this time,  $\xi/\xi(0)$  has decayed to approximately  $\frac{1}{2}$ . This process takes about 66 days. After the eddy has formed over the constant slope region beyond  $x = 200$  km,  $\xi/\xi(0)$  remains fairly constant. (The vorticity was averaged over the area enclosed by the depth contour at 80% of the central maximum depth of the eddy.)

(unbroken) current, the slope ( $S$ ) must be steeper than a critical value ( $S_c$ ) given by

$$S_c = \alpha f(H/g')^{1/2}, \tag{5.1}$$

where  $H$  is the current's maximum thickness,  $g'$  the "reduced gravity" and  $\alpha$  is a coefficient of order unity whose value depends on the distribution of potential vorticity (it is unity for uniform potential vorticity current and  $\sqrt{2}$  for zero potential vorticity flow).

2. When the slope ( $S$ ) is greater than  $S_c$ , the current flows continuously along the slope (Fig. 6a, left panel). However, when the slope is smaller than  $S_c$ , a steady continuous solution does not exist because the forward slope-induced speed is not strong enough to overcome the negative speed introduced along the inshore front. As a result, a chain of isolated eddies

propagating along the isobaths is established (Fig. 6a, right panel).

3. The scale of the eddies is given by,

$$\left(\frac{32Q}{\rho S f}\right)^{1/3},$$

where  $Q$  is the outflow's mass flux,  $S$  the bottom slope and  $f$  the Coriolis parameter. (For an outflow such as the Red Sea with  $Q$  of 0.3 Sv, an  $S$  of 0.02 and an  $f$  of  $10^{-5} \text{ s}^{-1}$ , the eddy radius is 25 km.)

4. The above eddy formation process is not related to the familiar instability-induced eddies because instability is, by definition, associated with the breakdown of a known steady solution and, in our case, a steady physically relevant solution does not exist.

Before proceeding, it should perhaps be stressed again that our conclusions are not inconsistent with those of Griffiths et al. (1982), Paldor and Killworth (1987) and Nof (1990) (who showed that, with the exception of frictionally dominated flows or very broad currents, all double frontal currents are unstable) because we are addressing an entirely different process. To illustrate this and to illustrate the fact that the basic current is stable, we have compared two currents with identical frictional coefficients but different bottom slopes (Fig. 6a). The two currents have the same frictional coefficient, the same initial potential vorticity (zero) and the same width. We showed that the current situated on the steep supercritical slope ( $S > S_c$ ) is stable and continuous (Fig. 6a). However, when the slope is gradually reduced (in the downstream direction) the current can no longer exist as a continuous current so it is replaced by a chain of isolated eddies propagating along the isobaths.

It is expected that most real outflows in the ocean will ultimately reach a point where they can no longer exist as a continuous current; beyond that point they can only exist as a chain of eddies. This is so because, as the outflow progresses away from the source, it entrains ambient fluid so that  $H$  increases and  $g'$  decreases. In view of (5.1), this means that, as one progresses away from the

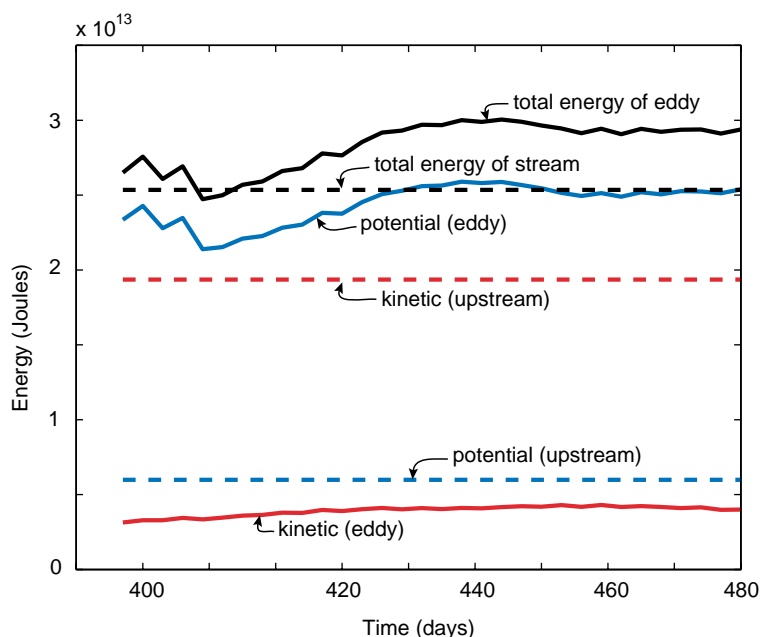


Fig. 10. Times evolution of the total energy (potential plus kinetic) of a typical eddy's core. The shown eddy is the same eddy shown earlier in Fig. 9, i.e., the eighth eddy generated in Exp. 19. The solid black line is the total energy of the eddy and the dashed black line is the total energy of an upstream (rectangular) strip ( $30 \text{ km} \times 571 \text{ km}$ ) with an identical volume. The solid blue line is the potential energy of the eddy and the solid red line is the eddy's kinetic energy. Their sum is the total energy of the eddy (solid black line). Similarly, the dashed blue line is the potential energy of the initial strip and the dashed red line is the kinetic energy of the initial strip. Note that, even though their vorticity is reduced by half during the experiment, the energy is nearly conserved. (There actually appears to be a slight increase in the energy but the increase is within the limits of our accuracy in tracing the eddy mass.) Interestingly, initially, most of the energy is associated with the kinetic energy whereas in the end most of the energy is potential (due to the doming associated with the establishment of the eddies). Also, note that, without performing a detailed tracing analysis, it is difficult to tell where the fluid contained in the final eddy originated from. It turns out, however, that, for the energy calculation, it does not make much difference where it originated from as the upstream energy does not vary that much across the stream.

source, one needs a steeper and steeper bottom in order to support the outflow as a continuous current. This condition is usually impossible to satisfy as the outflows tend to lose height due to energy loss (via frictional effects) so that as they proceed forward and get closer to the ocean bottom, they sense (due to the geography) a *smaller* rather than a larger slope.

Our results are applicable to many outflows but those of primary interest here are the Red Sea outflow and its counterpart, the Mediterranean outflow. Following Meschanov and Shapiro (1998) and Shapiro and Meschanov (1991) who noted that the density anomaly associated with Reddies was almost undetectable, we take for the Red Sea outflow away from the Straits of Bab-el-Mandeb, a very small density difference of

$\Delta\rho/\rho = 2 \times 10^{-6}$ ,  $f = 0.2 \times 10^{-4} \text{ s}^{-1}$ , and  $H \sim 200 \text{ m}$ . We find that, for these values, the critical slope  $S_c$  is fairly large, about 0.06. A somewhat larger density difference of  $4 \times 10^{-4}$  gives a somewhat smaller critical slope of 0.015. It is very difficult to say for certain whether the actual slope in the ocean is greater or smaller than these values particularly due to the variable slope, the ridges, troughs and fractured rifts (Fig. 1).

Immediately to the east of the Straits of Bab-el-Mandeb, the slope appears to be considerably smaller than the above values, about 0.005, implying that the outflow will be immediately decomposed into eddies (provided that it is immediately diluted to the density considered above). Farther downstream, on the other hand, the slope is perhaps as large as 0.01 and this could

perhaps sustain some sort of a continuous outflow. We, therefore, cannot unequivocally say whether the outflow consists of a chain of eddies due to our eddy-maker mechanism (i.e., the subcritical small slope). We can, however, state that the above values strongly suggest that this is a possibility. Finally, for a comparison, it is useful to apply the eddy-maker criteria to the Mediterranean outflow. For this outflow, the density anomaly is much greater than that of the Red Sea outflow and amounts to as much as  $\Delta\rho/\rho \sim 10^{-3}$ . However, the Coriolis parameter is also greater ( $10^{-4} \text{ s}^{-1}$ ) so that the critical slope is roughly the same as before, 0.015. It so happens that this is a typical slope for the region of interest implying that part of the topography may contain slopes that are either larger or smaller. This suggests that the eddy-making mechanism may or may not be active in the Mediterranean outflow.

Several additional comments should be made before closing. First, for simplicity, we have neglected the effects of friction in the development of the analytical theory. This is most likely not an entirely justified approximation particularly due to the role of bottom friction (see e.g., Borenäs and Wåhlin, 2000; Borenäs et al., in press; Wåhlin, 2002; Wåhlin and Walin, 2001) but an examination of this point is left for future investigations. Second, it is important to realize that, once formed, the eddies continue to propagate along the sloping bottom. In the Gulf of Aden–Indian Ocean system they are probably detached by an advective current which carries them to the middle of the ocean. Third, since it is hard to tell what portion of the outflow senses a subcritical or supercritical slope, the “chain” of eddies may consist of merely one eddy (if the region of a subcritical slope is of the length scale of the eddy). In this context the reader is referred to an animation ([www.doronnof.net/features.html#video](http://www.doronnof.net/features.html#video)) where the generation and merging of slope-induced eddies is vividly displayed. Fourth, the minimal number of observed Reddies can result from a limited region of subcritical slope, a limited occurrence of advective currents, and/or a short lifetime (due to small density signature and proximity to the western boundary). Fifth, it is important to realize that the  $\beta$ -induced westward

speed of the Reddies is negligible (due to a small density signature) compared to the advective currents in the region.

In summary, we offer a new eddy-generation mechanism which is unrelated to the classical eddy-generation process associated with instabilities. We offer it merely as a (yet unproved) possibility for Reddies, Meddies and other outflow-generated eddies.

### Acknowledgements

Discussions with A. Bower were very useful. Two anonymous reviewers provided helpful comments. This study was supported by the Binational Science Foundation under grant 96-105; National Science Foundation contract OCE 9911324; National Aeronautics and Space Administration grants NAG5-7630, NGT5-30164 and NAG5-10860; and Office of Naval Research grant N00014-01-0291. Drawings were done by Beth Raynor.

### References

- Armi, L., Zenk, W., 1984. Large lenses of highly saline Mediterranean water. *Journal of Physical Oceanography* 14, 1560–1576.
- Armi, L., Hebert, D., Oakey, N., Price, J.F., Richardson, P.L., Rossby, H.T., Ruddick, B., 1989. Two years in the life of a Mediterranean salt lens. *Journal of Physical Oceanography* 19, 354–370.
- Baines, P.G., Condie, S.A., 1998. Observations and modelling of Antarctic downslope flows. In: Jacobs, S.S., Weiss, R. (Eds.), *Ocean, Ice and Atmosphere: Interactions at the Antarctic Continental Margin*. American Geophysical Union, Washington, DC, pp. 24–29.
- Bleck, R., Boudra, D., 1986. Wind-driven spin-up in eddy-resolving ocean models formulated in isopycnic and isobaric coordinates. *Journal of Geophysical Research* 91, 7611–7621.
- Borenäs, K., Wåhlin, A., 2000. Limitations of the streamtube model. *Deep-Sea Research I* 47, 1333–1350.
- Borenäs, K., Wåhlin, A., Ambar, I., Serra, N. The Mediterranean outflow splitting—an intercomparison between theoretical models and CANIGO data. *Deep-Sea Research II*, in press.
- Borisov, S., Nof, D., 1998. Deep, cross-equatorial eddies. *Geophysical and Astrophysical Fluid Dynamics* 87, 273–310.

- Bower, A.S., Armi, L., Ambar, I., 1995. Direct evidence of Meddy formation off the southwestern coast of Portugal. *Deep-Sea Research I* 42, 1621–1630.
- Bower, A.S., Hunt, H.D., Price, J.F., 2000. Character and dynamics of the Red Sea and Persian Gulf outflows. *Journal of Geophysical Research* 105, 6387–6414.
- Cherniawsky, J., LeBlond, P.H., 1986. Rotating flows along indented coastlines. *Journal of Fluid Mechanics* 169, 379–407.
- Condie, S.A., 1995. Descent of dense water masses along continental slopes. *Journal of Marine Research* 53, 865–928.
- Csanady, G.T., 1979. The birth and death of a warm-core ring. *Journal of Geophysical Research* 84, 777–780.
- D'Asaro, E., 1988. Generation of submesoscale vortices: a new mechanism. *Journal of Geophysical Research* 93, 6685–6694.
- Ebbesmeyer, C., Taft, B.A., McWilliams, J.C., Shen, C.Y., Riser, S.C., Rossby, H.T., Biscayne, P.E., Ostlund, H.G., 1986. Detection, structure and origin of extreme anomalies in a western Atlantic oceanographic section. *Journal of Physical Oceanography* 16, 591–612.
- Flierl, G., 1979. A simple model of the structure of warm and cold-core rings. *Journal of Geophysical Research* 84, 78–85.
- Flierl, G., 1987. Isolated eddy models in geophysics. *Annual Review of Fluid Mechanics* 19, 493–530.
- Griffiths, R.W., 1986. Gravity currents in rotating systems. *Annual Review of Fluid Mechanics* 18, 59–89.
- Griffiths, R.W., Linden, P.F., 1981. The stability of vortices in a rotating, stratified fluid. *Journal of Fluid Mechanics* 105, 283–316.
- Griffiths, R.W., Linden, P.W., 1982. Laboratory experiments on fronts. Part 1: density-driven boundary currents. *Geophysical and Astrophysical Fluid Dynamics* 19, 159–187.
- Griffiths, R.W., Hopfinger, E.J., 1983. Gravity currents moving along a lateral boundary in a rotating fluid. *Journal of Fluid Mechanics* 134, 357–399.
- Griffiths, R.W., Killworth, P., Stern, M., 1982. Ageostrophic instability of ocean currents. *Journal of Fluid Mechanics* 117, 343–377.
- Hebert, D., Oakey, N., Rudduck, B., 1990. Evolution of a Mediterranean salt lens: scalar properties. *Journal of Physical Oceanography* 20, 1468–1483.
- Käse, R.H., Beckmann, A., Hinrichsen, H.H., 1989. Observational evidence of salt lens formation in the Iberian Basin. *Journal of Geophysical Research* 94, 4905–4912.
- Klinger, B., 1994a. Baroclinic eddy generation at a sharp corner in a rotating system. *Journal of Geophysical Research* 99, 12515–12531.
- Klinger, B., 1994b. Inviscid current separation from rounded capes. *Journal of Physical Oceanography* 24, 1805–1811.
- Lane-Serff, G., Baines, P., 1998. Eddy formation by dense flows on slopes in a rotating fluid. *Journal of Fluid Mechanics* 363, 229–252.
- McDowell, S.E., Rossby, H.T., 1978. Mediterranean water: an intense mesoscale eddy off the Bahamas. *Science* 202, 1085–1087.
- McWilliams, J., 1985. Submesoscale, coherent vortices in the ocean. *Reviews of Geophysics* 23, 165–182.
- McWilliams, J., 1988. Vortex generation through balanced adjustment. *Journal of Physical Oceanography* 18, 1178–1192.
- Meschanov, S.L., Shapiro, G.I., 1998. A young lens of Red Sea water in the Arabian Sea. *Deep-Sea Research I* 45, 1–13.
- Nof, D., 1983. The translation of isolated cold eddies on a sloping bottom. *Deep-Sea Research I* 30, 171–182.
- Nof, D., 1990. The breakup of dense filaments. *Journal of Physical Oceanography* 20, 880–889.
- Nof, D., 1991. Lenses generated by intermittent currents. *Deep-Sea Research I* 38, 325–345.
- Nof, D., Borisov, S., 1998. Inter-hemispheric oceanic exchange. *Quarterly Journal of the Royal Meteorological Society* 124, 2829–2866.
- Orlanski, I., 1976. A simple boundary condition for unbounded hyperbolic flows. *Journal of Computational Physics* 21, 251–269.
- Pichevin, T., Nof, D., 1997. The momentum imbalance paradox. *Tellus* 49, 298–319.
- Paldor, N., Killworth, P., 1987. Instabilities of a two-layer coupled front. *Deep-Sea Research I* 34, 1525–1539.
- Prater, M., Sanford, T., 1994. A meddy off Cape Saint Vincent; I, Description. *Journal of Physical Oceanography* 24, 1572–1586.
- Price, J.F., Baringer, M.O., Lueck, R.G., Johnson, G.C., Ambar, I., Parilla, G., Cantos, A., Kennelly, M.A., Sanford, T.B., 1993. Mediterranean outflow mixing dynamics. *Science* 259, 1277–1282.
- Richardson, P.L., Walsh, D., Armi, L., Schröder, M., Price, J.F., 1989. Tracking three Meddies with SOFAR floats. *Journal of Physical Oceanography* 19, 371–383.
- Røed, L.P., 1980. Curvature effects on hydraulically driven inertial boundary currents. *Journal of Fluid Mechanics* 90, 395–412.
- Shapiro, G., Meschanov, S.L., 1991. Distribution and spreading of Red Sea Water and salt lens formation in the northwest Indian Ocean. *Deep-Sea Research I* 38, 21–34.
- Spall, M., Price, F.J., 1998. Mesoscale variability in Denmark Strait: the PV outflow hypothesis. *Journal of Physical Oceanography* 28, 1598–1623.
- Spall, M., Richardson, P., Price, J., 1993. Advection and eddy mixing in the Mediterranean salt tongue. *Journal of Marine Research* 51, 797–818.
- Stern, M., 1980. Geostrophic fronts, bores, breaking and blocking waves. *Journal of Fluid Mechanics* 99, 687–703.
- Stern, M., Whitehead, J.A., 1990. Separation of a boundary jet in rotating fluid. *Journal of Fluid Mechanics* 217, 41–69.
- Stern, M., Whitehead, J.A., Hua, B.L., 1982. The intrusion of a density current along the coast of a rotating fluid. *Journal of Fluid Mechanics* 123, 237–265.

- Swaters, G.E., 1991. On the baroclinic instability of cold-core coupled density fronts on a sloping continental shelf. *Journal of Fluid Mechanics* 224, 361–382.
- Wåhlin, A., 2002. Topographic steering of dense bottom currents with application to submarine canyons. *Deep-Sea Research I* 49, 305–320.
- Wåhlin, A., Walin, G., 2001. Downward migration of dense bottom currents. *Environmental Fluid Mechanics* 1 (2), 41–69.
- Whitehead, J.A., Stern, M.E., Flierl, G.R., Klinger, B.A., 1990. Experimental observations of baroclinic eddies on a sloping bottom. *Journal of Geophysical Research* 95, 9585–9610.